[Lys^{40}(Ahx-DTPA-^{111}In)NH$_2$]Exendin-4, a Very Promising Ligand for Glucagon-like Peptide-1 (GLP-1) Receptor Targeting

Damian Wild[1], Martin Béhé[2], Andreas Wicki[3], Daniel Storch[4], Beatrice Waser[5], Martin Gotthardt[2], Boris Keil[6], Gerhard Christofori[3], Jean Claude Reubi[5], and Helmut R. Mäcke[4]

[1]Clinic and Institute of Nuclear Medicine, University Hospital Basel, Basel, Switzerland; [2]Department of Nuclear Medicine, Hospital of the Philipps-University, Marburg, Germany; [3]Institute of Biochemistry and Genetics, Center for Biomedicine, University of Basel, Basel, Switzerland; [4]Division of Radiological Chemistry, University Hospital Basel, Basel, Switzerland; [5]Institute of Pathology, University of Bern, Bern, Switzerland; and [6]Department of Radiology, Hospital of the Philipps-University, Marburg, Germany

High levels of glucagon-like peptide-1 (GLP-1) receptor expression in human insulinomas and gastrinomas provide an attractive target for imaging, therapy, and intraoperative tumor localization, using receptor-avid radioligands. The goal of this study was to establish a tumor model for GLP-1 receptor targeting and to use a newly designed exendin-4–DTPA (DTPA is diethylenetriaminepentaacetic acid) conjugate for GLP-1 receptor targeting. **Methods:** Exendin-4 was modified C-terminally with Lys^{40}-NH$_2$, whereby the lysine side chain was conjugated with Ahx-DTPA (Ahx is aminohexanoic acid). The GLP-1 receptor affinity (50% inhibitory concentration [IC$_{50}$] value) of [Lys^{40}(Ahx-DTPA)NH$_2$]exendin-4 as well as the GLP-1 receptor density in tumors and different organs of Rip1Tag2 mice were determined. Rip1Tag2 mice are transgenic mice that develop insulinomas in a well-defined multistage tumorigenesis pathway. This animal model was used for biodistribution studies, pinhole SPECT/MRI, and SPECT/CT. Peptide stability, internalization, and efflux studies were performed in cultured β-tumor cells established from tumors of Rip1Tag2 mice. **Results:** The GLP-1 receptor affinity of [Lys^{40}(Ahx-DTPA)NH$_2$]exendin-4 was found to be 2.1 ± 1.1 nmol/L (mean ± SEM). Because the GLP-1 receptor density in tumors of Rip1Tag2 mice was very high, a remarkably high tumor uptake of 287 ± 62 %IA/g (% injected activity per gram tissue) was found 4 h after injection. This resulted in excellent tumor visualization by pinhole SPECT/MRI and SPECT/CT. In accordance with in vitro data, [Lys^{40}(Ahx-DTPA-^{111}In)NH$_2$]exendin-4 uptake in Rip1Tag2 mice was also found in nonneoplastic tissues such as pancreas and lung. However, lung and pancreas uptake was distinctly lower compared with that of tumors, resulting in a tumor-to-pancreas ratio of 13.6 and in a tumor-to-lung ratio of 4.4 at 4 h after injection. Furthermore, in vitro studies in cultured β-tumor cells demonstrated a specific internalization of [Lys^{40}(Ahx-DTPA-^{111}In)NH$_2$]exendin-4, whereas peptide stability studies indicated a high metabolic stability of the radiopeptide in β-tumor cells and human blood serum. **Conclusion:** The high density of GLP-1 receptors in insulinomas as well as the high specific uptake of [Lys^{40}(Ahx-DTPA-^{111}In)NH$_2$]exendin-4 in the tumor of Rip1Tag2 mice indicate that targeting of GLP-1 receptors in insulinomas may become a useful imaging method to localize insulinomas in patients, either preoperatively or intraoperatively. In addition, Rip1Tag2 transgenic mice represent a suitable animal tumor model for GLP-1 receptor targeting.

Key Words: glucagon-like peptide-1 receptor; insulinoma; exendin-4; transgenic mouse model; ^{111}In

J Nucl Med 2006; 47:2025–2033

Peptide hormone receptors are expressed at high levels in a wide variety of human malignant tumors (*1*). Like other cellular surface molecules, these receptors have become increasingly important as targets for drugs. In particular, they allow tumor imaging and therapy with corresponding radiolabeled peptide hormone analogs. Among several receptors, somatostatin receptors were the first to be identified for in vivo targeting and are currently the clinically most widely applied ones. Indeed, because of its very high sensitivity and specificity, somatostatin receptor scintigraphy with [^{111}In-DTPA^0]octreotide (DTPA is diethylenetriaminepentaacetic acid) (OctreoScan; Mallinckrodt Medical) has become an integral part of the routine diagnostic work-up of patients with gastroenteropancreatic neuroendocrine tumors (*2*). DOTA-conjugated derivatives (DOTA is 1,4,7,10-tetraazacyclododecane-1,4,7,10-tetraacetic acid) of octreotide are being successfully introduced in targeted radionuclide therapy if labeled with ^{90}Y or ^{177}Lu (*3–6*). The latest generation of somatostatin analogs shows an improved receptor-binding profile, thereby extending the spectrum of targeted tumors and the possibility of labeling with the positron emitter ^{68}Ga for PET (*7,8*). Initial clinical results using the PET tracer [^{68}Ga-DOTA^0,1-Nal^3]octreotide clearly demonstrate a diagnostic improvement compared with [^{111}In-DTPA^0]octreotide (*9,10*).

Received Jun. 15, 2006; revision accepted Aug. 14, 2006.

For correspondence or reprints contact: Helmut R. Mäcke, PhD, Division of Radiological Chemistry, University Hospital Basel, Petersgraben 4, CH-4031 Basel, Switzerland.

E-mail: hmaecke@uhbs.ch

As the clinical results for somatostatin receptor targeting are encouraging, it has been important to identify novel peptide hormone receptors suitable for in vivo tumor targeting, with the aim of eventually targeting a wider range of malignant tumors as well as targeting individual tumors more efficiently using a cocktail of peptide analogs directed at multiple peptide receptors. Peptide receptors of current interest include bombesin receptors (*11–13*), cholecystokinin receptors (*14,15*), and others. A novel very promising candidate in this field is glucagon-like peptide-1 receptor (GLP-1 receptor), a member of the secretin receptor family (*16*). GLP-1 is known to be a potent glucose-dependent insulinotropic hormone that has important actions on gastric motility, on the suppression of plasma glucagon levels, and probably on the promotion of satiety and stimulation of glucose disposal in peripheral tissue independent of the actions of insulin. In addition, GLP-1 receptor was shown to be highly overexpressed in human insulinomas and gastrinomas (*17*). In insulinomas, the density of the GLP-1 receptor is considerably higher than that of any other peptide receptors, including somatostatin receptors. The mean receptor density in 25 specimen was found to be 8,133 ± 1,829 disintegrations per min/mg (dpm/mg) for the GLP-1 receptor, compared with 3,807 ± 2,521 dpm/mg for the somatostatin receptor subtype 2 (sst_2). The incidence of sst_2 and GLP-1 receptors in insulinomas is 18 per 26 and 25 per 27, respectively (*17*). In contrast to other neuroendocrine tumors, many insulinomas do express the sst_2 receptor often in very low density (*17*). As a consequence of the relatively low sst_2 expression, the sensitivity of detecting insulinomas is only 40%–60% (*18,19*). Other approaches including MRI, CT, arteriography, and sonography have been used. However, the diagnosis and localization of insulinomas remains a challenge because of the small size (<2 cm) of 90% of insulinomas (*20*). Therefore, GLP-1 receptor targeting of insulinomas might be a very promising new approach. First preclinical data demonstrated specific targeting of ^{125}I-labeled GLP-1(7–36) amide and ^{125}I-labeled exendin-3 in a mouse model bearing a subcutaneously implanted rat insulinoma tumor (RINm5F) (*21*). However, the low peptide stability of ^{125}I-labeled GLP-1 and the low efficiency of radioiodination of exendin-3 are limiting their clinical use. On the basis of the GLP-1 analog exendin-4, a new DTPA conjugate was synthesized for GLP-1 receptor targeting (*22*).

The goal of this study was to establish Rip1Tag2 mice as an in vivo tumor model for GLP-1 receptor targeting and to use the newly designed exendin-4–DTPA conjugate labeled with ^{111}In for GLP-1 receptor targeting. Rip1Tag2 transgenic mice express large-T antigen of simian virus 40 under the control of the rat insulin promoter and subsequently develop tumors of the pancreatic β-cells in a highly reproducible multistage tumor progression pathway (*23*). It is well known that human pancreatic β-cells express GLP-1 receptors (*24,25*). Therefore, we determined the GLP-1 receptor density in Rip1Tag2 tumor tissue by in vitro receptor autoradiography with ^{125}I-labeled GLP-1 as radioligand. Using this tumor model and a tumor cell line derived from it, we investigated internalization, cellular retention, biodistribution, and pharmacokinetics of the new radiopeptide ([Lys^{40}(Ahx-DTPA-^{111}In)NH_2]exendin-4) (Ahn is aminohexanoic acid).

MATERIALS AND METHODS

Abbreviations of the common amino acids are in accordance with the recommendations of the International Union of Pure and Applied Chemistry–International Union of Biochemistry Commission of Biochemical Nomenclature (Commission on Biological Nomenclature) (*26*).

Reagents and Instrumentation

All chemicals were obtained from commercial sources; GLP-1 and exendin-4 were from Bachem and were used without further purification. [Lys^{40}(Ahx-DTPA)NH_2]exendin-4 was custom-synthesized by Peptide Specialty Laboratories. The peptide conjugate was characterized by matrix-assisted laser desorption ionization-mass spectrometry (MALDI-MS) measurements that were done on a Voyager sSTR equipped with a Nd:YAG laser (355 nm) (Applied BioSystems). $^{111}InCl_3$ and ^{125}I-labeled GLP-1 were obtained from Mallinckrodt Medical and Anawa, respectively. For quantification of autoradiograms, a computer-assisted image-processing system was used (*27,28*) with tissue standards for iodinated compounds (Amersham). Analytic reversed-phase high-performance liquid chromatography (RP-HPLC) was performed on a Bischof HPLC system (Metrohm AG) with HPLC pumps 2250 and a λ-1010 ultraviolet detector (Metrohm AG) using CC250/4 Nucleosil 120-3 C_{18} columns from Macherey-Nagel. The gradient systems consisted of mixtures of water with 0.1% trifluoroacetic acid (TFA) (solvent A) and acetonitrile (solvent B): Gradient I: 0 min 95% A (5% B), 5 min 95% A (5% B), 10 min 0% A (100% B), 15 min 0% A (100% B), 20 min 95% A (5% B); flow, 0.75 mL/min; λ = 214 nm; and gradient II: 0 min 95% A (5% B), 30 min 55% A (45% B), 32 min 0% A (100% B), 34 min 0% A (100% B), 37 min 95% A (5% B); flow, 0.75 mL/min; λ = 214 nm. Quantitative γ-counting was performed on a COBRA 5003 γ-system well counter from Packard Instruments. The cell culture medium was Dulbecco's modified Eagle medium (DMEM high glucose, pH 7.4) supplemented with 10% fetal bovine serum, 2% L-glutamine, and 1% penicillin-streptomycin from Gibco BRL. Rip1Tag2 mice were scanned in an MR scanner (Magnetom Expert; Siemens) and with an e.cam SPECT scanner (Siemens) that was modified with a multipinhole aperture (*29*). SPECT images were reconstructed using HiSPECT reconstruction program (SciVis). Afterward, MRI and SPECT images were manually fused on a HERMES workstation (HERMES Medical Solutions). In addition, hybrid SPECT/CT scans (Symbia T2; Siemens) were performed. The coregistered CT scan was performed with intravenous contrast medium (Telebrix 30 meglumine; Megluminioxitalamat, 300 mg/mL [Guerbet]). Images were displayed and analyzed on the Syngo (Siemens) computer system.

Radiolabeling of [Lys^{40}(Ahx-DTPA)NH_2]Exendin-4 with $^{111}InCl_3$

An aliquot of 5 μL (0.2 mmol/L) [Lys^{40}(Ahx-DTPA)NH_2]exendin-4 was dissolved in 200 μL sodium acetate buffer (0.4 mol/L, pH 5.0). After adding 100 MBq $^{111}InCl_3$, the solution was incubated at room

temperature for 30 min and then subjected to quality control by analytic HPLC (gradient I).

Animal Model

Animals were maintained, treated, and cared for in compliance with guidelines of the Swiss regulations (approval 789). Rip1Tag2 transgenic mice were used for biodistribution studies, pinhole SPECT/MRI, and SPECT/CT. Additionally, C57BL/6J mice (wild type of Rip1Tag2 mice) were used as the control animals.

In Vitro GLP-1 Receptor Autoradiography

GLP-1 receptor autoradiography was used to detect and quantify the GLP-1 receptors in mouse tumor, pancreas, lung, and kidney samples. As reported previously (*17*), 20-μm-thick sections were incubated for 2 h at ambient temperature in the presence of 32 pmol/L ^{125}I-labeled GLP-1 (74 TBq/mmol [2,000 Ci/mmol]). The incubation solution was 170 mmol/L Tris-HCl buffer (pH 8.2) containing 1% bovine serum albumin, bacitracin (40 μg/mL), and $MgCl_2$ (10 mmol/L) to inhibit endogenous proteases. Nonspecific binding was determined by adding 100 nmol/L solution of unlabeled GLP-1. Incubated sections were washed twice for 5 min in cold incubation buffer containing 0.25% bovine serum albumin, then washed in buffer alone, and dried quickly. Finally, the sections were apposed to Biomax MR films (Kodak) and exposed for 1 wk in x-ray cassettes.

In selected cases, displacement experiments were performed on successive tissue sections using increasing concentrations of GLP-1, exendin-4, and the [Lys^{40}(Ahx-DTPA)NH_2]exendin-4 analog to measure their respective binding affinity to GLP-1 receptors.

In all experiments, the autoradiograms were quantified using a computer-assisted image processing system, as described previously (*27,28*). Tissue standards for iodinated compounds were used for this purpose.

Cell Culture, Radioligand Internalization, Externalization, and Peptide Stability Studies

GLP-1 receptor–expressing β-tumor cells were established from β-cell tumors of Rip1Tag2 mice. Tumors were homogenized and cells were initially kept in high-glucose DMEM containing 10% fetal calf serum and 10% heat-inactivated horse serum. Tumor cells were slowly expanded over 3 wk and then maintained by serial passage in monolayers in DMEM in a humidified 5% CO_2/air atmosphere at 37°C. Cell numbers were counted under a microscope with a Neubauer's counting chamber. For all cell experiments, the cells were seeded at a density of 0.8–1 million cells per well in 6-well plates and incubated overnight with internalization buffer (DMEM, 1% fetal bovine serum, amino acids, and antibiotics, pH 7.4) to obtain good cell adherence. The internalization rate was linearly corrected to 1 million cells per well in all experiments.

The medium was removed from the 6-well plates and the cells were washed once with 2 mL internalization buffer. To each well, 1.2 mL internalization buffer were added and incubated at 37°C for about 1 h. To the medium, 0.25 pmol [Lys^{40}(Ahx-DTPA-^{111}In)NH_2]exendin-4 was added (final concentration, 0.17 nmol/L). Then the cells were incubated at 37°C for the indicated periods of time.

Peptide concentration–dependent internalization was studied using 3 different concentrations of [Lys^{40}(Ahx-DTPA-^{111}In)NH_2]exendin-4 (0.17, 1.7, and 6.67 nmol/L). To determine nonspecific membrane binding and internalization, cells were incubated with the radioligand in the presence of 0.33 μmol/L unlabeled [Lys^{40}(Ahx-DTPA)NH_2]exendin-4.

Cellular uptake was stopped by removing the medium and by washing the cells twice with 1 mL ice-cold phosphate-buffered saline (PBS). An acid wash with a glycine buffer (pH 2.8) on ice was performed twice for 5 min to distinguish between membrane-bound (acid-releasable) and internalized (acid-resistant) radioligand. Finally, cells were treated with 1 mol/L NaOH. The culture medium, the receptor-bound fraction, and the internalized fraction were measured radiometrically in a γ-counter.

For cellular retention studies, β-tumor cells (0.8–1 million) were incubated with 0.25 pmol per well (0.17 nmol/L) [Lys^{40}(Ahx-DTPA-^{111}In)NH_2]exendin-4 for 120 min; then the medium was removed and the wells were washed twice with 1 mL ice-cold PBS. In each experiment, an acid wash with a glycine buffer (pH 2.8) on ice was performed twice for 5 min to remove the receptor-bound ligand. Cells were then incubated at 37°C with fresh internalization buffer. At different time points, the external medium was removed for quantification of radioactivity in a γ-counter and replaced with fresh medium. Finally, cells were solubilized in 1 mol/L NaOH, and the internalized radioactivity was quantified in a γ-counter. The recycled fraction was expressed as the percentage of the totally internalized radiopeptide per 1 million cells, and the integrity of the externalized peptide after 1- and 2-h externalization was determined using RP-HPLC (gradient II).

Peptide stability was determined after incubation of 7 pmol [Lys^{40}(Ahx-DTPA-^{111}In)NH_2]exendin-4 in 3 mL fresh human blood serum for at least 24 h. After certain time points, samples of 100 μL blood serum were taken and added to 200 μL methanol. After centrifugation, the radioactivity in the serum protein pellet and the supernatant was quantified in a γ-counter. Potential metabolites were analyzed by subjecting the supernatant to analytic HPLC (gradient II).

Biodistribution in Rip1Tag2 Mice

Rip1Tag2 and C57BL/6J mice (78- to 99-d old) were injected into the tail vein with 2 pmol (10 ng peptide/185–370 kBq) [Lys^{40}(Ahx-DTPA-^{111}In)NH_2]exendin-4 in a 100-μL 1% human serum albumin solution diluted in 0.9% NaCl. At 1, 4, 24, and 48 h after injection, mice were sacrificed under isoflurane and CO_2 anesthesia. Organs, blood, and tumors were collected, blotted dry, and weighed, and the radioactivity in these samples was determined using a γ-counter. The percentage of injected activity (%IA) was calculated for each tissue. Instead of measuring the radioactivity in a γ-counter, small samples of tumor, pancreas, lung, and kidney were snap frozen on dry ice and prepared for autoradiography.

To determine the nonspecific uptake of the radiopeptide, mice were coinjected with 2 pmol [Lys^{40}(Ahx-DTPA-^{111}In)NH_2]exendin-4 and 2 nmol [Lys^{40}(Ahx-DTPA-^{nat}In)NH_2]exendin-4 in a total volume of 100 μL 1% human serum albumin solution and sacrificed 4 h after injection.

GLP-1 Receptor Imaging with Multipinhole SPECT/MRI

Rip1Tag2 mice were injected with 37 MBq [Lys^{40}(Ahx-DTPA-^{111}In)NH_2]exendin-4 (50 pmol) into the tail vein. Four hours after injection, multipinhole SPECT images of Rip1Tag2 mice were performed under isoflurane anesthesia in prone position (*29*). Images were taken from 60 angles with a minimum of 30 kilocounts per angle, and image reconstruction was done by HiSPECT. Shortly thereafter, Rip1Tag2 mice were scanned in an MR scanner in the same prone position. To enhance the

signal-to-noise ratio, a specially designed and modified small-animal saddle coil was used. Coronal high-resolution slices were obtained using a 3-dimensional (3D) double echo in steady-state sequence. Transversal slices were reconstructed from the 3D dataset to obtain slices for image fusion. Reconstructed transverse MRI and SPECT images were manually fused using the anatomic information obtained from both imaging modalities. After imaging, in both animals necropsy was performed and the size of tumors was measured.

GLP-1 Receptor Imaging with SPECT/CT

Rip1Tag2 mice were injected with 27.8 MBq [Lys^{40}(Ahx-DTPA-^{111}In)NH_2]exendin-4 (40 pmol) as described. One hour after injection of the radiopeptide, 100 μL of contrast medium were injected into the tail vein. Then mice were sacrificed and bilateral nephrectomy was performed. During nephrectomy a drop of contrast medium (about 1 μL) was directly injected into the tumor for tumor visualization on the CT scan. Mice were then placed under a dual-head γ-camera with an integrated CT scanner, and SPECT images were obtained in a continuous mode. The angular range was 180° per γ-camera head and the acquisition time was 25 s per frame. The image matrix was 256 × 256, and images were reconstructed as 5-mm-thick sections by using an iterative algorithm. The CT data from the SPECT/CT examination were reconstructed in the transverse plane as 1-mm-thick sections. The following parameters were used for imaging: 130 kV, 80 mA·s, 1.5 s per rotation, and a table speed of 1 mm/s. All images were viewed with software that provided multiplanar reformatted images of SPECT, CT, and fused data with linked cursors. After imaging, selected organs and the tumor were collected and the radioactivity was determined using a γ-counter. Finally, the size of the tumor was measured with a caliper.

RESULTS

Synthesis and Radiolabeling

DTPA was coupled via the Lys side chain of the C-terminally extended exendin-4 using Ahx as the spacer between DTPA and the peptide. The composition and structural identity of [Lys^{40}(Ahx-DTPA)NH_2]exendin-4 was verified by analytic HPLC and MALDI-MS (calculated mass: 4,799.4 g; observed mass: 4,801.3 g ([M+2H]$^+$, 100%; 2,402.1 g [M+4H]$^{2+}$, 20%)). The labeling yield of [Lys^{40}(Ahx-DTPA-^{111}In)NH_2]exendin-4 was >99% at a specific activity of 90 GBq/μmol and a radiochemical purity of >90%. The HPLC elution time on different gradient systems was 11.33 min (gradient I) and 29.5 min (gradient II).

Expression of GLP-1 Receptors in Mouse Insulinoma Tumors

Receptor autoradiography revealed a very high density of GLP-1 receptors homogeneously distributed in the tumor sample. Conversely, the adjacent exocrine pancreas expressed only a very low level of receptors (Fig. 1). The mean density of the GLP-1 receptor was quantified and found to be extremely high, amounting to 17,269 ± 1,906 dpm/mg tissue (n = 5; mean ± SEM) compared with lung and kidney.

GLP-1 Receptor Binding Affinity for [Lys^{40}(Ahx-DTPA)NH_2]Exendin-4

High-affinity GLP-1 receptor binding was measured for [Lys^{40}(Ahx-DTPA)NH_2]exendin-4 in competition experiments. An IC_{50} value of 2.1 ± 1.1 nmol/L (mean ± SEM, n = 4) was found for [Lys^{40}(Ahx-DTPA)NH_2]exendin-4, compared with 0.65 ± 0.1 nmol/L (mean ± SEM, n = 11) for exendin-4 and 2.4 ± 0.1 nmol/L for GLP-1 (mean ± SEM, n = 3) using ^{125}I-labeled GLP-1 as radioligand.

In Vitro Internalization Studies in β-Tumor Cells

[Lys^{40}(Ahx-DTPA-^{111}In)NH_2]exendin-4 showed a linear uptake within 4 h of incubation in established β-tumor cells (Fig. 2A). Between 85% and 97% of totally internalized radioligand was specifically internalized. At 1 h, the specific uptake into β-tumor cells was 2.4% ± 0.4% of the totally administered activity, increasing to 9.8% ± 0.9% at 4 h. The time–activity curve did not show a plateau during the first 24 h of internalization (data not shown). The percentage of internalized peptide measured at 1 h as a function of injected radiopeptide concentrations is shown in Figure 2B.

Cellular Retention

The kinetics of externalization was studied with β-tumor cells exposed to the radiopeptide for 2 h. Within 4 h, only 23% ± 3% of the radioligand were released from the β-tumor cells and the externalization curve showed a flattening (Fig. 3). The externalized radioactivity represented intact peptide as identified by HPLC.

Stability in Human Serum

For the determination of peptide stability, [Lys^{40}(Ahx-DTPA-^{111}In)NH_2]exendin-4 was incubated in human blood serum at 37°C. After 4.5 h incubation, the protein fraction

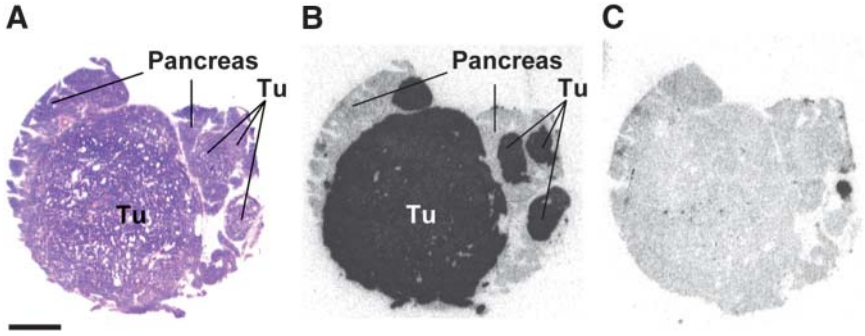

FIGURE 1. GLP-1 receptors in tumors of Rip1Tag2 mice: receptor autoradiographic illustration of GLP-1 receptors in tumors (Tu) and pancreas of a representative example. (A) Hematoxylin–eosin staining. (B) Autoradiogram shows total binding of ^{125}I-labeled GLP-1 in tumors and pancreas. (C) Autoradiogram shows nonspecific binding in presence of 100 nmol/L GLP. Bar = 0.1 mm.

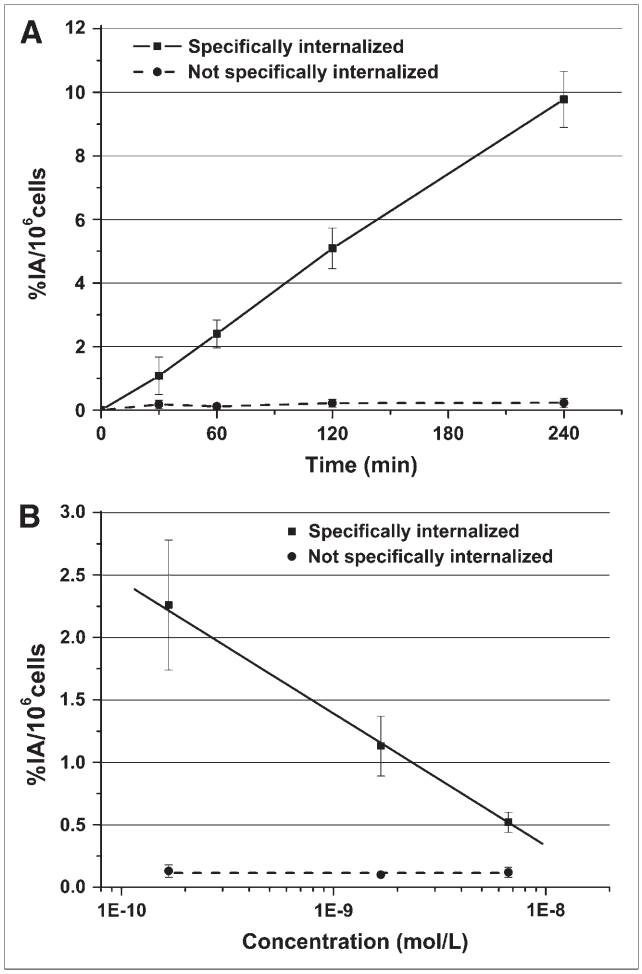

FIGURE 2. Specific (■) and nonspecific (●) internalization rates of [Lys^{40}(Ahx-DTPA-^{111}In)NH$_2$]exendin-4 into β-tumor cells. Values and SD are result of 2–4 independent experiments (triplicates in each experiment) and are expressed as percentage of activity internalized into 1 million cells. (A) In vitro kinetic of [Lys^{40}(Ahx-DTPA-^{111}In)NH$_2$]exendin-4 at 0.17 nmol/L peptide concentration. (B) Radiopeptide concentration–dependent specific internalization at 60 min.

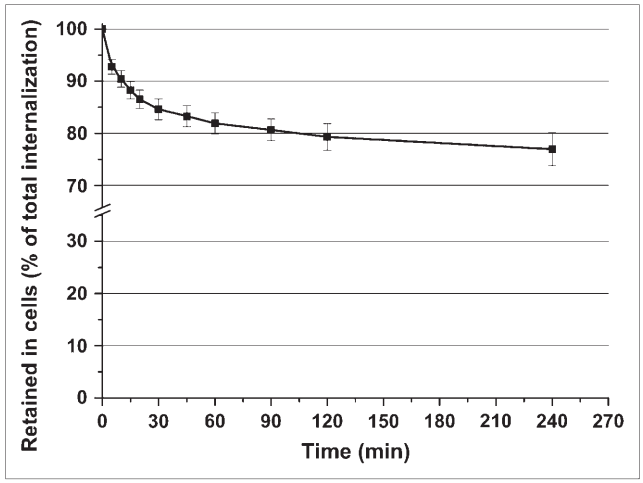

FIGURE 3. Externalization rate ± SD of [Lys^{40}(Ahx-DTPA-^{111}In)NH$_2$]exendin-4 after internalization for 120 min. Retained fraction is expressed as percentage of totally internalized radiopeptide per 1 million cells.

obtained as a pellet contained ≤6% of radioactivity and increased to 14.8% at 24 h. The supernatant was analyzed by analytic HPLC and showed 82.1% of intact peptide after 4.5 h and 73.7% after 24 h (Fig. 4).

Animal Biodistribution Studies

The levels of [Lys^{40}(Ahx-DTPA-^{111}In)NH$_2$]exendin-4 uptake, determined 4, 24, and 48 h after injection, in kidneys, liver, spleen, femur, and blood as well as in GLP-1 receptor–positive organs (lung, pancreas, stomach, and tumor) are shown in Table 1. Blood clearance was fast with 0.3 %IA/g remaining in blood 4 h after injection, resulting in very high tumor-to-normal organ ratios, especially tumor-to-blood ratios. By contrast, the organ and tumor excretion rate of the radiopeptide was slow. The accumulated activity in organs with the highest uptake, including kidneys, lung, pancreas, liver, and tumor, was 81% ± 9.1% of the totally injected activity at 4 h.

Four hours after injection of 2 pmol [Lys^{40}(Ahx-DTPA-^{111}In)NH$_2$]exendin-4 the uptake in the tumors (tumor weight, 5.6 ± 3.6 mg) was very high with 287 ± 62 %IA/g tissue. Only the uptake in the kidneys (209 ± 35 %IA/g) was nearly as high as in the tumors. Blocking with 1,000 times excess of cold ligand reduced the tumor uptake by >95%, whereas the kidney uptake was not affected. The tumor-to-kidney ratio was 1.38 at 4 h and 1.27 at 48 h. An important value for diagnostic use of [Lys^{40}(Ahx-DTPA-^{111}In)NH$_2$]exendin-4 is the tumor-to-pancreas ratio, which was 13.6 at 4 h and 9.71 at 48 h. One hour after injection, only weak and unspecific uptake was found in the lymphatic reticular tissue, such as spleen (2.6 ± 1 %IA/g) and bone marrow (1.5 ± 0.3 %IA/g).

A comparison of radiopeptide uptake in tumor, blood, and organs of Rip1Tag2 mice and wild-type C57BL/6J

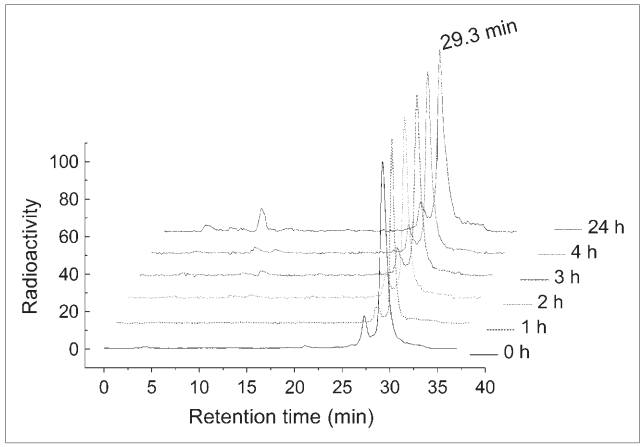

FIGURE 4. Stability of [Lys^{40}(Ahx-DTPA-^{111}In)NH$_2$]exendin-4 in human serum. After centrifugation, supernatant was analyzed on analytic HPLC at different time points.

TABLE 1
Biodistribution and Tissue Radioactivity Ratio in Tumor-Bearing Rip1Tag2 Mice at 4, 24, and 48 Hours After Injection of 2 pmol [Lys^{40}(Ahx-DTPA-^{111}In)NH_2]Exendin-4

		[Lys^{40}(Ahx-DTPA-^{111}In)NH_2]exendin-4	
Organ	Time (h)	Nonblocked (%IA/g)	Blocked* (%IA/g)
Lung	4	65.08 ± 18.62	0.86 ± 0.04†
	24	51.58 ± 4.25	
	48	31.21 ± 2.73	
Pancreas	4	21.13 ± 7.35	1.44 ± 0.43†
	24	20.05 ± 4.29	
	48	13.59 ± 0.47	
Stomach	4	4.68 ± 0.73	0.72 ± 0.23†
	24	2.86 ± 0.25	
	48	2.75 ± 0.53	
Tumor	4	287.37 ± 62.37	7.28 ± 3.50†
	24	181.82 ± 81.77	
	48	132.01 ± 41.04	
Kidneys	4	208.77 ± 34.68	214.91 ± 4.71
	24	148.16 ± 35.98	
	48	104.10 ± 15.04	
Liver	4	0.97 ± 0.27	0.35 ± 0.09
	24	0.68 ± 0.10	
	48	0.53 ± 0.07	
Spleen	4	1.55 ± 0.73	1.77 ± 0.31
	24	1.18 ± 0.16	
	48	0.91 ± 0.14	
Bone	4	0.40 ± 0.13	0.07 ± 0.04
	24	0.30 ± 0.08	
	48	0.42 ± 0.19	
Blood	4	0.29 ± 0.22	0.16 ± 0.03
	24	0.10 ± 0.01	
	48	0.06 ± 0.01	

	[Lys^{40}(Ahx-DTPA-^{111}In)NH_2]exendin-4	
Ratio	4 h after injection	48 h after injection
Tumor/blood	991	2,200
Tumor/kidneys	1.38	1.27
Tumor/lung	4.42	4.23
Tumor/pancreas	13.6	9.71

*Blocked with 2 nmol [Lys^{40}(Ahx-DTPA-^{nat}In)NH_2]exendin-4.
†GLP-1 receptor–positive organs.
Values are given as %IA/g tissue ± SD.

mice is shown in Figure 5. In all normal organs, the uptake in the transgenic mice was the same as that in the wild-type mice.

In Vivo GLP-1 Receptor Imaging

Iteratively reconstructed multipinhole SPECT/MR images were performed to visualize tumors in Rip1Tag2 transgenic mice 4 h after injection of 37 MBq [Lys^{40}(Ahx-DTPA-^{111}In)NH_2]exendin-4 (Fig. 6). In pinhole SPECT, 5 small pancreatic tumors (1–3.2 mm) and both kidneys were visible. Other GLP-1 receptor–positive organs, such as lung (M. Körner, M. Stöckli, R.C. Reubi, oral communication, 2006) and pancreas (*30*) were not detectable. In contrast to high-resolution MRI, pinhole [Lys^{40}(Ahx-DTPA-^{111}In)NH_2]exendin-4 SPECT visualized small insulinoma tumors with a maximal diameter of 1 mm (Fig. 6).

In comparison with pinhole SPECT, the resolution of ordinary SPECT is limited. Nevertheless, iteratively reconstructed SPECT/CT images of Rip1-Tag2 mice 1 h after injection of 27.8 MBq [Lys^{40}(Ahx-DTPA-^{111}In)NH_2]exendin-4 demonstrated very high uptake exclusively in the tumor after bilateral nephrectomy (Fig. 7).

DISCUSSION

This study describes the preclinical evaluation of a DTPA linker–conjugated exendin-4 derivative for the labeling with the γ- and Auger-emitter ^{111}In and the targeting

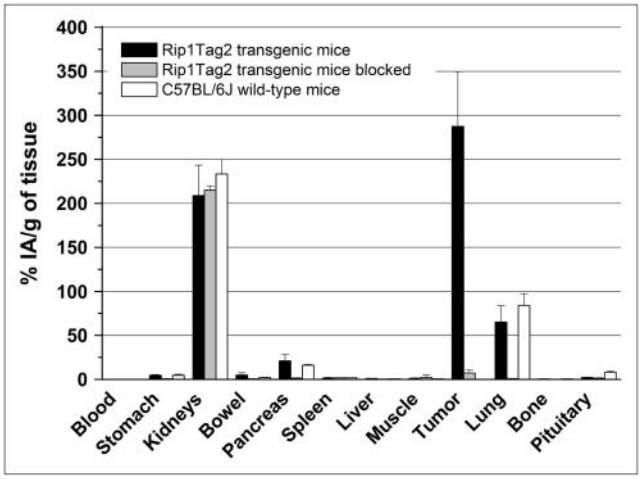

FIGURE 5. Biodistribution of [Lys^{40}(Ahx-DTPA-^{111}In)NH_2]exendin-4 in C57BL/6J wild-type mice and tumor-bearing Rip1Tag2 mice 4 h after injection of radiopeptide. Values and SD are result of 2 independent experiments with a total of 6 Rip1Tag2 mice (black and gray bars) and 3 wild-type mice (white bars). Gray bars show uptake in tumors and organs of Rip1Tag2 mice after coinjection with excess cold peptide.

of GLP-1 receptor–positive tumors in the Rip1Tag2 transgenic mouse model of pancreatic β-cell carcinogenesis.

The main rationale to develop a radiopeptide for the targeting of the GLP-1 receptor is based on the need to develop tools for imaging and localization of insulinomas

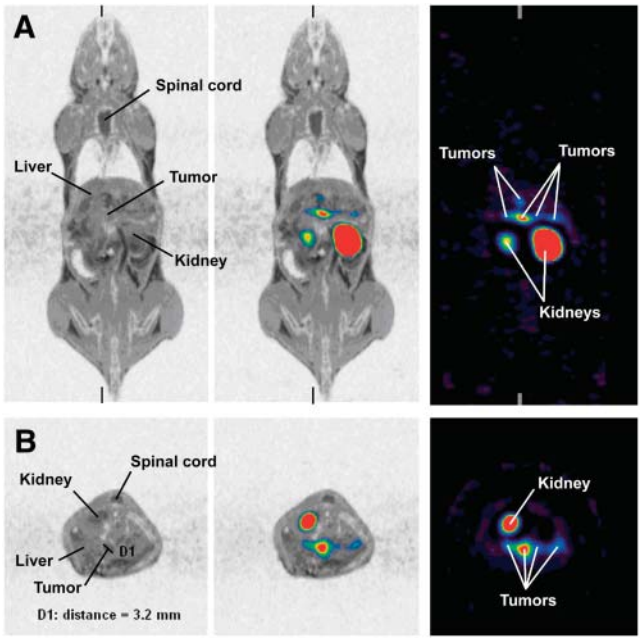

FIGURE 6. GLP-1 receptor imaging in a tumor-bearing Rip1Tag2 mouse 4 h after injection of [Lys^{40}(Ahx-DTPA-^{111}In)NH_2]exendin-4. (A) Coronal MR image (left), multipinhole SPECT/MR fusion image (center), and multipinhole SPECT image (right). (B) In corresponding transversal sections, maximal tumor diameter in MR image is 3.2 mm. In the MR image, only the largest tumor is visible—in contrast to the pinhole SPECT image, where 4 additional small tumors are apparent.

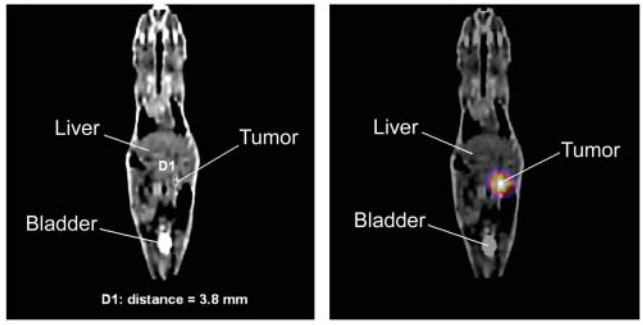

FIGURE 7. (Right) Coronal SPECT/CT image of a tumor-bearing Rip1Tag2 mouse 1 h after injection of [Lys^{40}(Ahx-DTPA-^{111}In)NH_2]exendin-4. (Left) Corresponding contrast medium–enhanced CT scan with tumor size of 3.8 mm. Tumor size measured with a caliper was $4.5 \times 3 \times 3$ mm.

by SPECT, PET, or use of a surgical probe for intraoperative localization.

Although sst_2 receptor targeting with radiopeptides is a very successful method for the diagnosis and therapy of neuroendocrine tumors, radiolabeled peptides have not been effective enough for a curative approach (*31*). In addition, about 50% of insulinomas are not detectable using [^{111}In-DTPA^0]octreotide because the sst_2 receptor density on the cell membrane is too low for visualization with [^{111}In-DTPA^0]octreotide (*18,19*). Therefore, detection of receptors expressed in higher density, leading to higher tumor uptake, is desirable. The GLP-1 receptor, which is expressed at high levels in human insulinomas, is such a promising receptor. In this regard, the Rip1Tag2 transgenic mouse model that develops insulinoma-like tumors appears to be an ideal tumor model to study and optimize different GLP-1/exendin-based radiopeptides. Indeed, an extremely high [Lys^{40}(Ahx-DTPA-^{111}In)NH_2]exendin-4 uptake of 287 ± 62 %IA/g tissue was found 4 h after injection in the tumor of Rip1Tag2 mice, which could be blocked by >95% when coinjected with a 1,000 times excess of cold peptide. To our knowledge, such a high specific tumor uptake has never been observed before in an animal model. There are different possible explanations for this: (a) the extremely high GLP-1 receptor density on the membrane of tumor cells as measured by autoradiography ($17{,}269 \pm 1{,}906$ dpm/mg tissue); (b) the high [Lys^{40}(Ahx-DTPA)NH_2]exendin-4 affinity to the GLP-1 receptor (50% inhibitory concentration [IC_{50}] = 2.1 ± 1.1 nmol/L); (c) the slow washout rate of the peptide found in vivo and in cultivated β-tumor cells; and (d) finally, the pronounced tumor angiogenesis in the Rip1Tag2 mouse model compared with xenograft-bearing mouse models might be an additional reason for the high uptake (*32*).

In addition, good results are expected in a clinical setting, as the GLP-1 receptor density in the Rip1Tag2 mouse insulinoma model is similar to that in human insulinomas.

Indium-111–coupled peptides are predominantly used for tumor imaging in the clinic, but recently ^{111}In was also proposed for therapeutic application using the radiotoxic

effect of Auger electrons (*33,34*). Therefore, [^{111}In-DTPA^{0}]octreotide was used for targeted radionuclide therapy of neuroendocrine tumors with encouraging results (*35*). Unfortunately, the dose-limiting factor was bone marrow toxicity. In the Rip1Tag2 mouse model, the bone marrow uptake 1 h after injection was 1.5 ± 0.3 %IA/g tissue, resulting in a favorable tumor-to-bone marrow ratio of 181. However, not only a very high tumor uptake but also a high kidney uptake was found in this animal model (tumor-to-kidney ratio 4 h after injection, 1.38). The high kidney uptake was not GLP-1 receptor mediated, as the uptake by kidneys could not be blocked by an excess of [Lys^{40}(Ahx-DTPA-^{nat}In)NH_2]exendin-4, suggesting that the accumulation of [Lys^{40}(Ahx-DTPA-^{111}In)NH_2]exendin-4 in the kidney tissue is most likely due to tubular cell reabsorption as found with most radiopeptides. However, patients with neuroendocrine tumors treated with a cumulative dose of 100 GBq [^{111}In-DTPA^{0}]octreotide showed no kidney toxicity at all (*35*). Therefore, kidney toxicity is not expected from diagnostic doses of [Lys^{40}(Ahx-DTPA-^{111}In)NH_2]exendin-4.

Previous in vivo studies used the ^{125}I-labeled GLP-1 (7–36) amide and ^{125}I-labeled exendin-3 for GLP-1 receptor targeting in a rat insulinoma model (RINm5F cells). The radiopeptides were shown to target specifically the xenografted tumor shortly after injection, yet the tumor-to-background ratio was low during the time period studied (*21*). Nevertheless, the tumor-to-background ratio is very important in case of diagnostic use of the radiopeptide. Insulinomas originate from pancreatic islet cells, whereas gastrinomas occur primarily in the gastrinoma triangle, defined as the confluence of the cystic and common bile duct, the second and third portions of the duodenum, and the neck and body of the pancreas. Therefore, the tumor-to-organ ratios—including normal pancreas, intestine, stomach, muscle, and liver—are important. In Rip1Tag2 mice, the tumor-to-organ ratio was very high for these organs at all time points (4 h after injection: tumor-to-pancreas ratio, 13.6; tumor-to-intestine ratio, 58; tumor-to-stomach ratio, 61; tumor-to-muscle ratio, 299; tumor-to-liver ratio, 296). The tumor-to-lung ratio (4.4 at 4 h) is relatively low in Rip1Tag2 mice. It is not known whether human lung expresses high densities of GLP-1 receptors. However, it is established that human pancreatic β-cells express high levels of GLP-1 receptors (*24,25*). Yet, because of their small size, pancreatic islets may not be visible within the pancreas on a SPECT scan.

Indeed, only multiple pancreatic tumors and both kidneys were visible on the pinhole SPECT, which was performed in Rip1Tag2 mice. The normal pancreatic tissue was not visible because the tumor-to-pancreas ratio was >10 in our animal model. In addition, pinhole SPECT visualized small tumors with a size of 1 mm because of high tumor uptake. However, on the MR scan of the same animal such small tumors were not visible, although a small animal saddle coil was used to enhance the signal-to-noise ratio. The main advantage of the multipinhole SPECT technique is the excellent resolution at the expense of sensitivity. However, pinhole SPECT is not often used on patients because sensitivity and short scan time are more important than a higher image resolution. Therefore, we performed additional SPECT scans with the same hybrid camera as that used for patients. As expected, a differentiation between tumor and kidney was not possible in these small animals. Nevertheless, the tumor with a size of only 4.5 × 3 × 3 mm was visible with a good contrast after bilateral nephrectomy. At a very high threshold level, only the lungs were distinguishable from the tumor with a weak signal. To confirm these findings the activity of relevant organs was measured with a γ-counter. One hour after injection, the absolute uptake in the kidneys was 35 %IA each, followed by the tumor (5.7 %IA) and the lung (1.0 %IA). These findings indicate that a small tumor (<5 mm) can be visualized by a normal SPECT camera if the absolute tumor uptake is high. Insulinomas are very difficult to visualize by any method because of their small size of <2 cm in 90% of the cases (*20*). Nevertheless, preoperative localization and staging are essential because of the possibility of multiple insulinomas, malignancy, and metastatic disease. In addition, many surgeons emphasize the importance of preoperative localization of insulinomas because these lesions cannot be identified during surgical exploration in 10%–20% of the cases (*36*). Hence, not only preoperative but also intraoperative tumor localization using a normal or endoscopic γ-probe might be an additional clinical application of radiolabeled exendin-4. The high density and incidence of GLP-1 receptors in insulinomas—the highest density of peptide receptors ever measured in cancers—suggest that the targeting of GLP-1 receptors in insulinomas may be considerably more promising than any other peptide receptor imaging method.

However, hardly any data exist on GLP-1 receptor expression in tumors other than neuroendocrine gut tumors: GLP-1 receptors were reportedly found in several tumor cell lines, including a human gastric cancer cell line (*37*), the rat pheochromocytoma cell line PC12 (*38*), and a rat medullary thyroid carcinoma cell line (*39*). Therefore, tissue from different tumors will have to be screened for GLP-1 receptors to evaluate the full clinical potential of GLP-1 receptor targeting.

CONCLUSION

The encouraging preclinical data of [Lys^{40}(Ahx-DTPA-^{111}In)NH_2]exendin-4 presented here warrant further studies on patients with this new radiopeptide for diagnostic imaging and intraoperative localization with a γ-probe. Coupling of exendin-4 to a DOTA chelator and labeling with ^{68}Ga may allow the use of this new peptide for PET and PET/CT and, if labeled with a β-, α-, or Auger electron-emitter, even for internal radiotherapy. Finally, Rip1Tag2 transgenic mice represent an animal tumor model with high GLP-1 receptor density and high reproducibility

and, therefore, represent a suitable animal model for studying comparative therapy protocols.

ACKNOWLEDGMENTS

The authors are grateful to Sibylle Tschumi and Roland Jost for technical support. This work was supported by the Swiss Cancer League (project OCS-01778-08-2005), the Swiss National Science Foundation (project 3100A0-100390), the European Molecular Imaging Laboratories, and the Roche Research Foundation.

REFERENCES

1. Reubi JC. Peptide receptors as molecular targets for cancer diagnosis and therapy. *Endocr Rev.* 2003;24:389–427.
2. Gibril F, Reynolds JC, Doppman JL, et al. Somatostatin receptor scintigraphy: its sensitivity compared with that of other imaging methods in detecting primary and metastatic gastrinomas—a prospective study. *Ann Intern Med.* 1996;125:26–34.
3. Waldherr C, Pless M, Maecke HR, et al. Tumor response and clinical benefit in neuroendocrine tumors after 7.4 GBq ^{90}Y-DOTATOC. *J Nucl Med.* 2002;43: 610–616.
4. Kwekkeboom DJ, Bakker WH, Kam BL, et al. Treatment of patients with gastro-entero-pancreatic (GEP) tumours with the novel radiolabelled somatostatin analogue [^{177}Lu-DOTA^0,Tyr^3]octreotate. *Eur J Nucl Med Mol Imaging.* 2003;30: 417–422.
5. Kwekkeboom DJ, Teunissen JJ, Bakker WH, et al. Radiolabeled somatostatin analog [^{177}Lu-DOTA^0,Tyr^3]octreotate in patients with endocrine gastroenteropancreatic tumors. *J Clin Oncol.* 2005;23:2754–2762.
6. Bodei L, Cremonesi M, Zoboli S, et al. Receptor-mediated radionuclide therapy with ^{90}Y-DOTATOC in association with amino acid infusion: a phase I study. *Eur J Nucl Med Mol Imaging.* 2003;30:207–216.
7. Wild D, Schmitt JS, Ginj M, et al. DOTA-NOC, a high-affinity ligand of somatostatin receptor subtypes 2, 3 and 5 for labelling with various radiometals. *Eur J Nucl Med Mol Imaging.* 2003;30:1338–1347.
8. Ginj M, Chen J, Walter MA, Eltschinger V, Reubi JC, Maecke HR. Preclinical evaluation of new and highly potent analogues of octreotide for predictive imaging and targeted radiotherapy. *Clin Cancer Res.* 2005;11:1136–1145.
9. Wild D, Macke HR, Waser B, et al. ^{68}Ga-DOTANOC: a first compound for PET imaging with high affinity for somatostatin receptor subtypes 2 and 5. *Eur J Nucl Med Mol Imaging.* 2005;32:724.
10. Baum RP, Niesen A, Leonhardi J, Wortmann R, Müller D, Rösch F. Receptor PET/CT imaging of neuroendocrine tumours using the Ga-68 labelled, high affinity somatostatin analogue DOTA-1-Nal^3-octreotide (DOTANOC): clinical results in 327 patients [abstract]. *Eur J Nucl Med Mol Imaging.* 2005;32(suppl 1):S54.
11. Zhang H, Chen J, Waldherr C, et al. Synthesis and evaluation of bombesin derivatives on the basis of pan-bombesin peptides labeled with indium-111, lutetium-177, and yttrium-90 for targeting bombesin receptor-expressing tumors. *Cancer Res.* 2004;64:6707–6715.
12. Smith CJ, Sieckman GL, Owen NK, et al. Radiochemical investigations of gastrin-releasing peptide receptor-specific [^{99m}Tc(X)(CO)$_3$-Dpr-Ser-Ser-Ser-Gln-Trp-Ala-Val-Gly-His-Leu-Met-(NH$_2$)] in PC-3, tumor-bearing, rodent models: syntheses, radiolabeling, and in vitro/in vivo studies where Dpr = 2,3-diaminopropionic acid and X = H$_2$O or P(CH$_2$OH)$_3$. *Cancer Res.* 2003;63: 4082–4088.
13. Van de Wiele C, Dumont F, Dierckx RA, et al. Biodistribution and dosimetry of ^{99m}Tc-RP527, a gastrin-releasing peptide (GRP) agonist for the visualization of GRP receptor-expressing malignancies. *J Nucl Med.* 2001;42:1722–1727.
14. Behr TM, Jenner N, Behe M, et al. Radiolabeled peptides for targeting cholecystokinin-B/gastrin receptor-expressing tumors. *J Nucl Med.* 1999;40:1029–1044.
15. Nock BA, Maina T, Behe M, et al. CCK-2/gastrin receptor-targeted tumor imaging with ^{99m}Tc-labeled minigastrin analogs. *J Nucl Med.* 2005;46:1727–1736.
16. Kieffer TJ, Habener JF. The glucagon-like peptides. *Endocr Rev.* 1999;20: 876–913.
17. Reubi JC, Waser B. Concomitant expression of several peptide receptors in neuroendocrine tumours: molecular basis for in vivo multireceptor tumour targeting. *Eur J Nucl Med Mol Imaging.* 2003;30:781–793.
18. Krenning EP, Kwekkeboom DJ, Bakker WH, et al. Somatostatin receptor scintigraphy with [^{111}In-DTPA-D-Phe^1]- and [^{123}I-Tyr^3]-octreotide: the Rotterdam experience with more than 1000 patients. *Eur J Nucl Med.* 1993;20:716–731.
19. Modlin IM, Tang LH. Approaches to the diagnosis of gut neuroendocrine tumors: the last word (today). *Gastroenterology.* 1997;112:583–590.
20. Gouya H, Vignaux O, Augui J, et al. CT, endoscopic sonography, and a combined protocol for preoperative evaluation of pancreatic insulinomas. *AJR.* 2003; 181:987–992.
21. Gotthardt M, Fischer M, Naeher I, et al. Use of the incretin hormone glucagon-like peptide-1 (GLP-1) for the detection of insulinomas: initial experimental results. *Eur J Nucl Med Mol Imaging.* 2002;29:597–606.
22. Gotthardt M, Lalyko G, Behr TM, Béhé M. Development of an ^{111}In-labeled GLP-1 analog for the scintigraphic diagnosis of neuroendocrine tumors [abstract]. *Eur J Nucl Med Mol Imaging.* 2005;46(suppl 2):91P.
23. Hanahan D. Heritable formation of pancreatic beta-cell tumours in transgenic mice expressing recombinant insulin/simian virus 40 oncogenes. *Nature.* 1985; 315:115–122.
24. Kreymann B, Williams G, Ghatei MA, Bloom SR. Glucagon-like peptide-1 7-36: a physiological incretin in man. *Lancet.* 1987;2:1300–1304.
25. Thorens B, Porret A, Buhler L, Deng SP, Morel P, Widmann C. Cloning and functional expression of the human islet GLP-1 receptor: demonstration that exendin-4 is an agonist and exendin-(9-39) an antagonist of the receptor. *Diabetes.* 1993;42:1678–1682.
26. IUPAC-IUB Commission of Biochemical Nomenclature (CBN) (1972). Symbols for amino-acid derivatives and peptides: recommendations 1971. *Eur J Biochem.* 1971;27:201–207.
27. Reubi JC, Laderach U, Waser B, Gebbers JO, Robberecht P, Laissue JA. Vasoactive intestinal peptide/pituitary adenylate cyclase-activating peptide receptor subtypes in human tumors and their tissues of origin. *Cancer Res.* 2000;60:3105–3112.
28. Reubi JC, Gugger M, Waser B, Schaer JC. Y(1)-mediated effect of neuropeptide Y in cancer: breast carcinomas as targets. *Cancer Res.* 2001;61:4636–4641.
29. Schramm NU, Ebel G, Engeland U, Schurrat T, Behe M, Behr TM. High-resolution SPECT using multi-pinhole collimation. *IEEE Trans Nucl Sci.* 2003;50: 315–320.
30. Mayo KE, Miller LJ, Bataille D, et al. International Union of Pharmacology: XXXV—the glucagon receptor family. *Pharmacol Rev.* 2003;55:167–194.
31. Krenning EP, Kwekkeboom DJ, Valkema R, Pauwels S, Kvols LK, De Jong M. Peptide receptor radionuclide therapy. *Ann N Y Acad Sci.* 2004;1014:234–245.
32. Bergers G, Hanahan D, Coussens LM. Angiogenesis and apoptosis are cellular parameters of neoplastic progression in transgenic mouse models of tumorigenesis. *Int J Dev Biol.* 1998;42:995–1002.
33. Behr TM, Behe M, Lohr M, et al. Therapeutic advantages of Auger electron-over beta-emitting radiometals or radioiodine when conjugated to internalizing antibodies. *Eur J Nucl Med.* 2000;27:753–765.
34. Chen P, Wang J, Hope K, et al. Nuclear localizing sequences promote nuclear translocation and enhance the radiotoxicity of the anti-CD33 monoclonal antibody HuM195 labeled with ^{111}In in human myeloid leukemia cells. *J Nucl Med.* 2006;47:827–836.
35. Valkema R, De Jong M, Bakker WH, et al. Phase I study of peptide receptor radionuclide therapy with [In-DTPA]octreotide: the Rotterdam experience. *Semin Nucl Med.* 2002;32:110–122.
36. Angelini L, Bezzi M, Tucci G, et al. The ultrasonic detection of insulinomas during surgical exploration of the pancreas. *World J Surg.* 1987;11:642–647.
37. Hansen AB, Gespach CP, Rosselin GE, Holst JJ. Effect of truncated glucagon-like peptide 1 on cAMP in rat gastric glands and HGT-1 human gastric cancer cells. *FEBS Lett.* 1988;236:119–122.
38. Perry T, Lahiri DK, Chen D, et al. A novel neurotrophic property of glucagon-like peptide 1: a promoter of nerve growth factor-mediated differentiation in PC12 cells. *J Pharmacol Exp Ther.* 2002;300:958–966.
39. Crespel A, De Boisvilliers F, Gros L, Kervran A. Effects of glucagon and glucagon-like peptide-1-(7-36) amide on C cells from rat thyroid and medullary thyroid carcinoma CA-77 cell line. *Endocrinology.* 1996;137:3674–3680.